https://doi.org/10.48048/tis.2022.5823

R-SFCL and RRCOCS-TVC Based Cooperative Control for Enhancing LVRT Capability of DFIG System

Md Sabbir Haider Khan[*] and Sanjeev Kumar Mallik

Department of Electrical Engineering, National Institute of Technology Patna, Patna, India

([*]Corresponding author's e-mail: mdk.phd16.ee@nitp.ac.in)

Received: 13 July 2021, Revised: 16 September 2021, Accepted: 23 September 2021

Abstract

For the extraction of wind energy through a doubly-fed induction generator (DFIG), low voltage ride through (LVRT) is an essential technical requirement specified by the transmission system operator (TSO). Under a grid fault condition, DFIG should remain in connection with the grid for a certain minimum period and offer reactive power support as required by the TSO. A cooperative control scheme consisting of hardware solution through a superconducting resistance type fault current limiter (R-SFCL) and software solution constructed on the rotor reference current orientation control strategy (RRCOCS) with transient voltage control (TVC), is proposed in this paper to address the LVRT requirement. In the proposed control strategy, RRCOCS will limit the rotor current directly during a fault condition. The reactive power needs to be generated during fault to maintain grid code which is achieved through TVC. At the same time, improvement of stator terminal voltage, as well as suppression of stator current, is achieved by R-SFCL. The suppression of stator current by R-SFCL is also transformed to the rotor side aiding the rotor current limiting. The proposed cooperative scheme's performance is simulated and tested on a 9 MW grid-connected DFIG wind system. The results obtained by the proposed strategy are compared with RRCOCS and RRCOCS-TVC.

Keywords: Wind energy conversion system, DFIG, Cooperative LVRT control, R-SFCL

Nomenclature

$\vec{u}_s$	Stator voltage vector	R_s	Stator resistance
$\vec{u}_r$	Rotor voltage vector	R_r	Rotor resistance
$\vec{i}_s$	Stator current vector	ω_s	Synchronous speed
$\vec{i}_r$	Rotor current vector	L_s	Stator self-inductance
$\vec{\psi}_s$	Stator flux linkage vector	L_r	Rotor self-inductance
$\vec{\psi}_r$	Rotor flux linkage vector	L_m	Mutual inductance between stator and rotor windings
S	Slip of the DFIG	ω_r	Rotor speed
$\vec{\psi}_{sdq}$	d-q stator flux components	$\vec{i}_{sdq}$	d-q stator current components
$\vec{\psi}_{rdq}$	d-q rotor flux components	$\vec{i}_{rdq}$	d-q rotor current components
$u_{r-a,b,c}$	Rotor 3-phase voltages	$u_{g-a,b,c}$	Three-phase voltages at the grid side of GSC
u_{gd}, u_{gq}	d-q components of the voltage at the grid side of GSC	i_{gd}, i_{gq}	d-q components of the current flowing amid GSC and grid
L_g	Filter inductance	T_{em}	Electromagnetic torque
p	The numerical value of pole pairs	T_m	Mechanical torque
J_{gen}	Equivalent inertia of the machine	Q_s	Stator reactive power

Q_g	Reactive power exchange through GSC	u_{rd}, u_{rq}	d-q rotor voltage components
U_{dc}	DC-link voltage	*	Reference values for the respective variables
τ_q	The time constant of the SFCL quenching interval	τ_r	The time constant of the SFCL reverse recovery interval
τ_{st}	The stator time constant of DFIG	R_{SFCL}	SFCL resistance
DFIG	Doubly-fed induction generator	WECS	Wind energy conversion system
LVRT	Low voltage ride through	TSO	Transmission system operator
R-SFCL	Superconducting resistance type fault current limiter	SFCL	Superconductive fault current limiter
BFCL	Bridge type fault current limiter	RSC	Rotor side converter
TVC	Transient voltage control	GSC	Grid side converter
DVS	Dynamic voltage stabilizer	DBR	Dynamic braking resistor
PCC	Point of common coupling	CBFCL	Capacitive bridge type fault current limiter
HTS	High-temperature superconductor	SCIG	Squirrel cage induction generator
GCSC	Gate controlled series capacitor	MPPT	maximum power point tracking
WT	Wind turbine	PWM	Pulse width modulation
FRT	Fault ride through	STATCOM	Static synchronous compensator
RRCOCS	Rotor reference current oriented control scheme		

Introduction

The doubly-fed induction generator (DFIG) has been extensively employed in the wind energy conversion system (WECS) due to its variable operating speed range, lower rating of converters, and flexibility in real power and reactive power control. In DFIG, the stator directly connects with the grid, and the power transfer from the stator to the grid is controlled via the rotor side converter (RSC). The grid side converter (GSC) controls the voltage of the dc bus installed between the power electronic converters. It is responsible for regulating the active and reactive power transfer between the grid and the rotor of DFIG [1]. Due to the growing penetration of wind-based power generation in the electric utility grid, WECS is needed to be investigated for the grid fault condition.

The DFIG's stator direct connection to the grid is a big concern for the power producers and utility grid during grid fault [2]. The voltage level at the grid connection point gets reduced during grid faults and results in a high transient stator current. This also has a detrimental effect on the rotor, since it is magnetically coupled to the stator, and contributes to the flow of large current in the rotor [3-6]. The rotor emf also increases and crosses the maximum permissible value under grid faults [7-9]. The high amount of the rotor circuit current and increased rotor emf of DFIG are responsible for the RSC failure and the dc-link voltage destabilization. Due to the failure of RSC, there is a complete loss of control of DFIG. The destabilized DC-link voltage reduces the capacitor life and also turns down the efficiency of power converters [10]. Moreover, the gearbox and bearings also face high mechanical stress due to torque oscillations and may worsen their lifespan [3-5].

WECS is constrained to fulfill a specific technical requirement in terms of grid codes for the transmission network's uninterrupted engagement as specified by the transmission system operator (TSO). Low voltage ride-through (LVRT) is one of the vital grid code requirements in which WECS must stay coupled to the grid even in the incident of fault for a specific minimum time and protect WECS from electrical and mechanical abnormalities [11]. The LVRT performance of DFIG-WECS may be enhanced using the software control method through the RSC of DFIG and modified hardware-based solutions. Several software schemes are proposed in the literature without modifying the reference current of the conventional control structure. A genetic algorithm-based optimally tuned LQR controller is proposed with an improved dynamic response when compared to a PI controller [12]. The controller performance was found robust to perturbation in stator voltage. Similarly, the authors have proposed a nonlinear sliding mode theory application in improving the LVRT of a DFIG-WECS [13]. The controller's performance was robust to perturbation in wind speed and machine parameters and proved to enhance the

LVRT ability during faults. Employment of a model predictive control (MPC) scheme has proved in improving the damping, accuracy, and speed of the controller to track reference currents during fault [14].

Software methods with modified reference current include a demagnetizing control designed to counteract the natural and negative components associated with transient flux [15]. A flux linkage control is realized to suppress overcurrent in the rotor circuit by regulating the flux produced in the rotor to trace the proportionate flux in the rotor [16]. RSC of DFIG emulates the characteristics of inductance and is proved in improving ride-through capability [17]. A rotor reference current orientation control strategy (RRCOCS) is proposed in which the current reference is modified for the rotor current loop by following an orientation scheme with the stator circuit current to overturn the rotor circuit high current and reduce the rotor emf [18]. The software control schemes [12-18] underperform under a severe grid fault condition. Due to extremely low voltage at the common coupling point (PCC) under a severe fault condition, the reactive power available to DFIG is not sufficient to support the voltage at the PCC [19].

The crowbar circuit is the most common hardware modification method applied when the current in the rotor circuit exceeds the permissible level [8]. However, DFIG with a crowbar circuit is similar to the caged induction generator (SCIG) and draws reactive power from the grid [20]. Dynamic braking resistor (DBR) in series is another cost-efficient approach for LVRT improvement of large wind farms [21]. Static compensator (STATCOM) [22], dynamic voltage stabilizer (DVS) [23], gate-controlled series capacitor (GCSC) [24] are some other proposed auxiliary hardware methods. These methods help to achieve better transient performance and compensate for the reduced PCC voltage. A bridge-type fault current limiter is proposed where the faulty current passes through a dc reactor and dissipating resistance and is proved in improving LVRT dynamics [25]. Another article has presented a fault current limiter with the capacitive bridge (CBFCL) for LVRT improvement. It has got improved merits over BFCL in terms of reactive power support, reduced complexity in the circuit, and reduced cost [26]. In recent a cascade converter-based LVRT control of DFIG is proposed which offers great current-limiting ability at a significantly reduced rating of auxiliary hardware device [27-28]. Hybrid hardware solutions (a combination of 2 hardware devices) are also proposed to give improved results [29-30]. Superconducting resistance fault current limiter (R-SFCL) with features of quick response, self-triggering, and self-recovery has been proved effective in enhancing the LVRT ability of DFIG-WECS by restraining the fault current [31]. Selecting a higher value for the current limiting resistance of SFCL can further improve the PCC voltage but it will also produce a significant amount of joule heating within the SFCL and increases the post fault recovery time. Moreover, it may cause overcompensation of the stator voltage and significantly high electromagnetic transients after fault removal [32].

The existing software and hardware methods operating alone have several limitations and the inability to meet the recent strict grid codes provided by the TSO. The recent software methods like RRCOCS [18] and TVC [19] offer a limited improvement restricted to small and moderate level grid faults when acting alone. Moreover, the DFIG critical variables surpass the safe limits, and DFIG fails to provide reactive power support during severe grid faults as required by TSO. On the other hand, R-SFCL will result in excessive Joule heating if an R-SFCL with a high resistance value is employed to satisfy the grid code [32]. This may damage R-SFCL and its superconducting property on a repeated number of operations. Also, the SFCL installed on the grid-tied lines cannot individually meet the limiting capacity for the rotor current of each DFIG in a wind farm. This article proposes a cooperative control technique merging with a hardware device and modified software schemes. In the proposed method an R-SFCL is first utilized to enhance the terminal voltage of DFIG and suppressing the grid currents. Improved software control methods (RRCOCS) and the transient voltage control (TVC) using RSC and GSC are then introduced to perk up the transient performance. RRCOCS is introduced for directly limiting the transient rotor current, TVC is exploited for reactive power generation. With a combination of R-SFCL, RRCOCS, and TVC control schemes, the proposed scheme can limit the rotor circuit over current, suppress the electromagnetic torque oscillations, and ensures that the terminal voltage at the PCC is sustained as per utility grid codes. Moreover, the requirement of R-SFCL current limiting resistance is significantly reduced.

This paper is structured as follows. At the first, the mathematical modeling of DFIG and control associated with the RSC and GSC of DFIG is presented. Then, the principle and topology of the proposed cooperative control scheme are illustrated. Also, the equivalent modeling of R-SFCL and its characteristics is explained followed by the modified control structure for DFIG converters. And in the end, the simulation results and performance evaluation are done followed by the conclusion.

Materials and methods

DFIG-WECS consists of a wind-driven turbine with its control unit, the wound rotor induction generator, and a set of 2 adjacent pulse width modulated (PWM) power electronic converters with its control structure. The generator is coupled to the grid using a step-up transformer as per the grid voltage level (Refer to **Figure 1**) [8]. The WECS control entails the turbine control and the converter control at 2 levels. Wind turbine control is performed first to determine the generator reference torque and pitch angle reference to meet several requirements; i.e., to extract maximum available energy from wind by MPPT, keep turbine within safe operational limits in terms of (power, speed, and torque) [1]. Converter control at the second level is used to generate the switching pattern of GSC and RSC using the reference generated by wind turbine control [1].

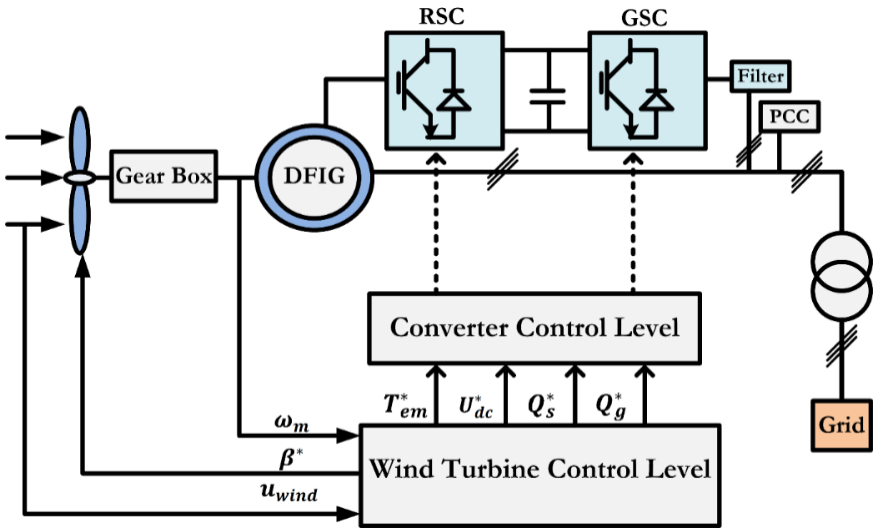

Figure 1 Schematic diagram of DFIG based WECS.

The converter control is based on traditional vector control applied on RSC and GSC. The control strategy at 2-level is therefore used for the optimization of power in the safe wind speed range. Also, it helps limit power production for abnormal wind speeds. Mathematical model development of DFIG is required for the realization of 2-level control strategies which is presented in the subsequent section.

DFIG mathematical model

Using the most common park model for induction generator [2], the stator and the rotor winding voltage vectors of DFIG in stationary reference frame can be expressed as:

$$\vec{u}_s = R_s \vec{i}_s + \frac{\partial \vec{\psi}_s}{\partial t} \tag{1}$$

$$\vec{u}_r = R_r \vec{i}_r + \frac{\partial \vec{\psi}_r}{\partial t} - j\omega_r \vec{\psi}_r \tag{2}$$

where $\vec{u}_s$, R_s and $\vec{\psi}_s$ are stator voltage vector, stator resistance, and stator flux linkage vector, respectively. Similarly, $\vec{u}_r$, R_r and $\vec{\psi}_r$ are rotor voltage vector, rotor resistance, and rotor flux linkage vector, respectively. The rotor speed is symbolically represented by ω_r.

The grid determines the stator voltage $\vec{u}_s$ as the stator is directly connected with the grid. PWM converter controls the rotor voltage to perform the desired power or torque control. The developed flux linkages around the stator and rotor windings of DFIG are given by:

$$\vec{\psi}_s = L_s\vec{i}_s + L_m\vec{i}_r \tag{3}$$

$$\vec{\psi}_r = L_r\vec{i}_r + L_m\vec{i}_s \tag{4}$$

where L_s, L_r and L_m are the stator circuit self-inductance, rotor circuit self-inductance, and mutual inductance between stator and rotor circuits, respectively.

The generator torque in synchronous (d-q) reference frame can be expressed as [1]:

$$T_{em} = p\frac{L_m}{L_s}\mathrm{Im}(\vec{\psi}_{sdq}\vec{i}^{*}_{rdq}) = p(\vec{\psi}_{sq}\vec{i}_{rd} - \vec{\psi}_{sd}\vec{i}_{rq}) \tag{5}$$

where p symbolizes the numerical value of poles in pairs.

Applying fundamental dynamic law on the generator's rotating part, rotor speed (ω_r) of the DFIG can be evaluated as:

$$J_{gen}\frac{d\omega_r}{dt} = T_m - T_{em} \tag{6}$$

where J_{gen} represents the inertia equivalent of the machine; T_{em} and T_m symbolizes electromagnetic torque and mechanical torque, respectively.

Vector control of DFIG

In the classical vector control approach of the DFIG, the power electronics converter is being controlled by the traditional PI controller using d-q transformation. The control stratagem for the converters, RSC, and the GSC are presented in **Figure 2**. RSC control is centered on the stator-voltage-oriented form of the vector control. The in effect decouple control is accomplished round the reasonably autonomous d-axis and q-axis controller loops using conventional PI controllers. This is realized by the alignment of the d-axis of the (d-q) frame of reference with the DFIG's stator voltage vector.

The generator torque and the reactive power flow in the stator can then be expressed as:

$$T_{em} = \frac{L_m}{L_s}\psi_{sq}i_{rd} \tag{7}$$

$$Q_s = \omega_s\frac{L_m}{L_s}\psi_{sq}i_{rq} - \omega_s\frac{\psi_{sq}}{L_s}\psi_{sq} \tag{8}$$

where ω_s is the synchronous frequency of the DFIG stator variables.

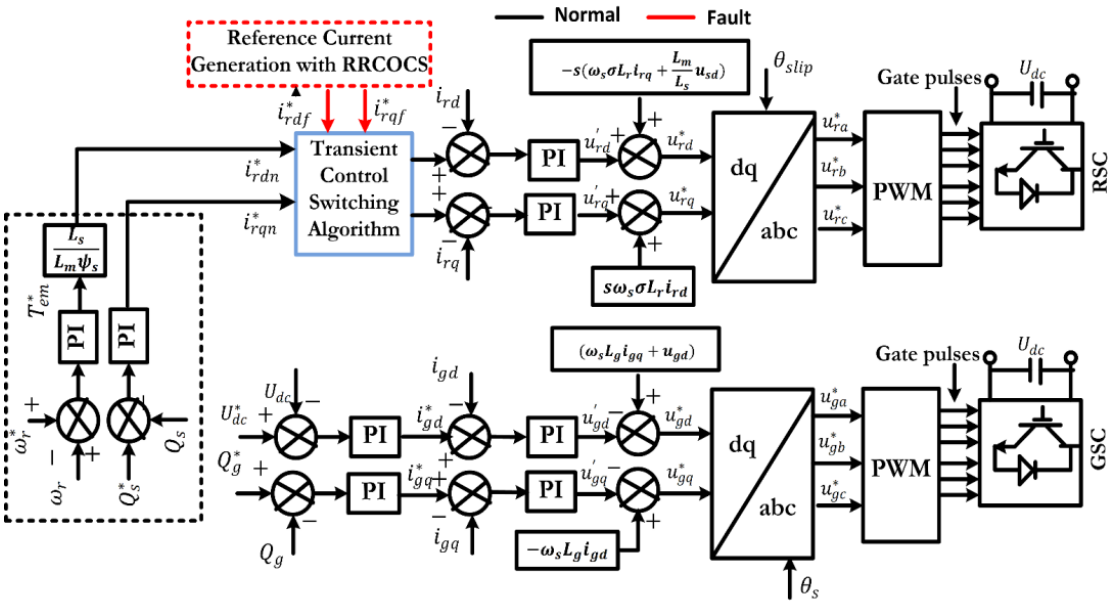

Figure 2 RSC and GSC control diagram incorporated with transient switching model of RRCOCS.

The generator torque and reactive power through the stator are directly proportional to d- and q-axis current in the rotor, respectively. The d axis current reference (i_{rd}^*) is yielded on regulating the reference torque (T_{em}^*) round the PI controller loop of rotor speed (ω_r). The value of reference rotor speed (ω_r^*) is evaluated using the maximum power point (MPPT) curve. The reference current (i_{rq}^*) for q-axis is generated by regulating stator reactive power (Q_s) as shown in **Figure 2**. By comparing i_{rd}^* and i_{rq}^* with the actual rotor currents i_{rd} and i_{rq}, the errors obtained are exercised as inputs to another set of PI regulators and generates a set of voltages $u_{rd}^{'}$ and $u_{rq}^{'}$. These voltages set are then recompensed using the cross-coupling terms $-s\omega_s\sigma L_r i_{rq}$, $s\omega_s\sigma L_r i_{rd}$ and feed-forward terms $s(L_m/L_s)u_{sd}$ to produce the reference voltage signal u_{rd}^* and u_{rq}^*. The d-q voltage references are then transformed to reference 3-phase voltage signals u_{ra}^*, u_{rb}^* and u_{rc}^* for the rotor, which passes through (PWM) block and breeds the switching pulses to drive the RSC.

The DC-link voltage (U_{dc}) is being regulated by GSC control regardless of the mode of operation of DFIG, i.e.; subsynchronous and super synchronous. Similar to the control structure of RSC, GSC control is realized by the orientation of the d-axis of the (d-q) frame of reference with the utility grid voltage vector. The voltage at the dc bus is proportional to (i_{gd}) i.e., the d-axis current amid grid and GSC. While the reactive power flowing amid GSC and the grid is relative to the q-axis current (i_{gq}). The currents i_{gd} and i_{gq} are regulated by controlling d-axis voltage (u_{gd}) and q-axis voltage (u_{gq}), respectively. The d-axis reference current (i_{gd}^*) is generated employing a PI regulator loop around the voltage at the dc-link. Likewise, the q- axis reference current (i_{gq}^*) is obtained from the controller loop over reactive power flowing through GSC (refer to **Figure 2**). It is generally preferred for DFIG to operate at unity power factor in normal conditions to minimize losses and exploit the active power transmission. Hence, the reference reactive power for both converters' control is tuned to zero.

The conventional Vector control performs well under normal operation. However, to protect the WECS and to improve the system's transient performance during fault events, it is required to introduce a

modified control structure and circuits. Several modified software control schemes and hardware methods have been evolved by the power system researcher. Cooperative hardware and modified software transient control scheme are purported in this paper for improving the performance during the fault.

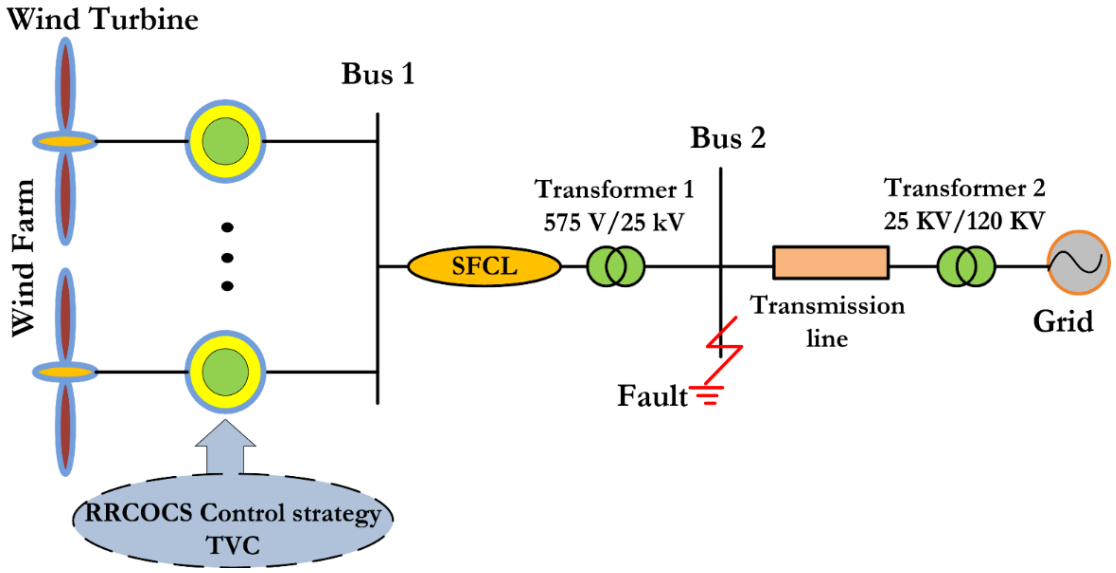

Figure 3 Schematic of the proposed cooperative control topology.

Cooperative control topology and principle

The schematic representation of the proposed cooperative control with a resistance type SFCL and 2 improved converter control methods of DFIG is shown in **Figure 3**. The wind farm system includes 6 wind turbines, each of 1.5 MW DFIGs connected to the grid. The DFIG parameters exercised in the simulation are given in **Table 1**.

The SFCL is installed in between the DFIG terminal (bus 1) and the (transformer1). The equivalent grid fault analysis model for the entire system under a test condition of the most severe 3 phases with ground fault is represented in **Figure 4** [32].

Table 1 Machine parameters used in the simulation.

DFIG parameters	Values
Rated power	1.5 MW
Nominal DFIG stator voltage	575 Volts, line-line
System power frequency	60 Hertz
Stator winding resistance (R_s)	23*10e-3 p.u.
Rotor winding resistance (R_r)	16*10e-3 p.u.
Magnetizing inductance (L_m)	2.9 p.u.
Pair of poles (p)	3
DC-link nominal voltage	1150 V
Rated torque	0.83 p.u.

From the basics of network loop analysis, the drop in voltage at bus 1 after the fault event is estimated as [32]:

$$\Delta\dot{U}_s \approx \left(\frac{Z_s}{Z_s + Z_{SFCL} + Z_{T1} + Z_g} - \frac{Z_f}{Z_f + Z_g} \times \frac{Z_s}{Z_s + Z_{SFCL} + Z_{T1}} \right) \times \dot{U}_g + \left(\frac{Z_{SFCL} + Z_{T1} + Z_g}{Z_s + Z_{SFCL} + Z_{T1} + Z_g} - \frac{Z_{SFCL} + Z_{T1} + Z_f}{Z_s + Z_{SFCL} + Z_{T1} + Z_f} \right) \times \dot{E}_g \tag{9}$$

where $\dot{E}_s$, Z_s are the transient stator voltage and the equivalent DFIG impedance; Z_{SFCL}, Z_{T1} represent the impedance offered by SFCL and the impedance of Transformer 1. $\dot{U}_g$, Z_g symbolize the grid voltage equivalent and its impedance, respectively. Z_f is the fault impedance.

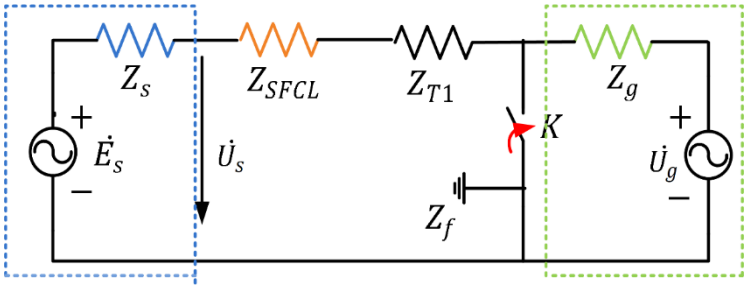

Figure 4 Equivalent fault analysis model of the test system under grid fault.

With the drop in voltage at Bus 1, the 3-phase to ground fault also roots a severe current flow through stator winding. The moment the stator winding current surpasses the critical current level of the SFCL tied in line, a self-operating SFCL starts quenching and increases its impedance to a sudden high value, and develops a fairly high voltage potential across the SFCL. This compensates for the drop in voltage and improves the voltage at Bus1 as evident from (9). Meanwhile, the RRCOCS and TVC control are exploited to protect the DFIG from over current and contribute reactive power to support the grid.

R-SFCL equivalent modeling

R-SFCL can be represented by a time-varying resistance whose characteristics can be depicted in **Figure 5**. Under normal operation of the grid up to time t_1, the SFCL offers zero resistance since the SFCL current is within the critical current limit. For the grid fault occurring at the time t_1, the overcurrent starts the quenching process and the SFCL finally reaches a state with high resistance at the time t_2.

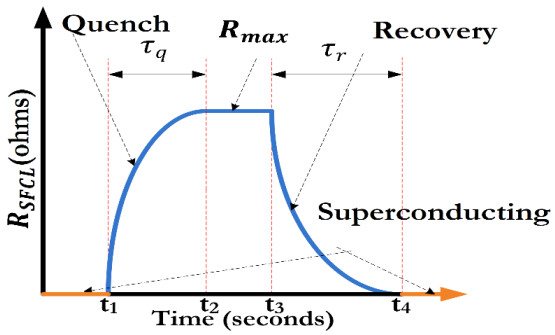

Figure 5 Resistance characteristics curve of SFCL.

After the grid fault disappearance at the time t_3, the SFCL comes back to the original superconducting state at the time t_4. The SFCL's resistance under different operating states can be expressed mathematically as:

$$R_{SFCL} = \begin{cases} R_{\max} \times \left[1 - \exp(-t/\tau_q)\right] & t_1 < t < t_2 \\ R_{\max} & t_2 < t < t_3 \\ R_{\max} \times \left[\exp(-t/\tau_r)\right] & t_3 < t < t_4 \end{cases} \quad (10)$$

where $R_{\max}$ is the maximum resistance offered by SFCL after completing the quenching process. τ_q and τ_r symbolizes the time constant of the quenching process and recovery process, respectively.

The triggering and state transition of SFCL is modeled in MATLAB/Sim power systems [32]. The voltage variation across SFCL owing to an instantaneous change in its resistance is imitated by a controlled voltage source dependent on fault current. This voltage is then inserted into the grid-connected line and mimics the fault current limiting effect of the SFCL. The voltage at Bus 1 changes for different values of SFCL resistance $(R_{\max})$ with SFCL acting alone [32]. It can be seen that for a larger $(R_{\max})$ value, a better improvement can be seen for the transient voltage at Bus 1 is following (9) theoretically.

Modified control scheme for DFIG converters

The use of SFCL based hardware method is coordinated with 2 modified control schemes for converters, TVC, and RRCOCS to improve the inclusive transient performance of WECS assuring the critical parameters remain within permissible limits and to bring improvement in terms of cost-saving and reduction in thermal losses associated with the SFCL device.

Transient voltage control (TVC)

The recent grid codes want the DFIG system to inject maximum reactive current into the utility grid once the PCC fault level is detected above 50 % [11]. This caters to reacting power generation. To integrate the participation of RSC and GSC for transient voltage improvement, a modified control scheme is developed by the power system researcher [19] and presented in **Figure 6**. In this control scheme the required reactive power regulation is shared automatically between the 2 converters owing to terminal voltage changes. Under the normal operating condition, TVC control is inactive. As soon as fault is detected, control loop is activated to regulate the terminal voltage through reactive power generation by DFIG utilizing excess energy available with the DC link. RSC and GSC control i_{sq} and i_{gq} respectively for generating reactive powers at the stator terminal and the GSC output terminal. However, i_{gq} is injected by the GSC only if the level of fault is high enough and RSC exceeds its capacity limit.

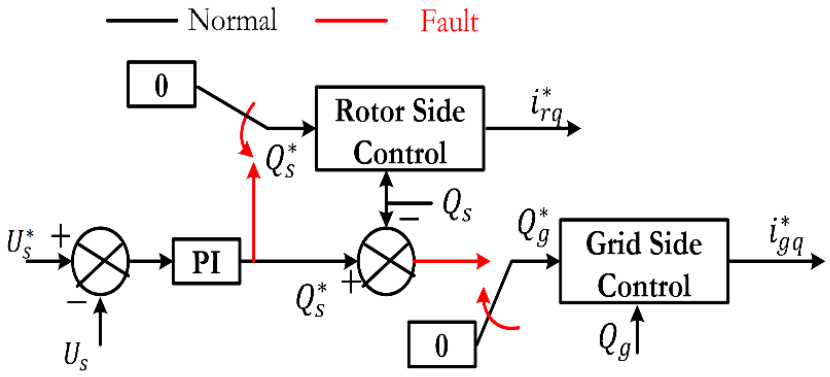

Figure 6 Converters control diagram with TVC capability.

RRCOCS control strategy

The RRCOCS control strategy is employed to reduce the rotor over-current and rotor emf during grid fault [18]. In this software-based scheme, the reference rotor current gets oriented with the stator current during fault episode. In the occurrence of a fault, the stator of DFIG experiences a dip in voltage level. The flux being a state variable, cannot experience any discontinuity [2]. The stator flux does not change to a new steady-state value at a sudden and evolves with a transient component known as natural flux along with the ac component called forced flux. Hence, the flux value at the instant of fault gets a sudden rise due to the presence of 2 components and slowly settles down to a new steady-state value.

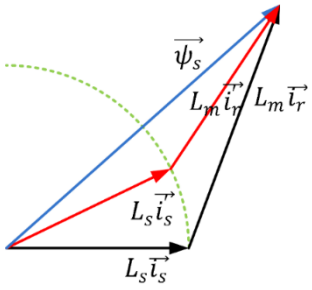

Figure 7 Phasor representation between stator-flux, stator circuit current, and rotor current.

Using (3), the relationship between stator currents, rotor currents, and stator flux has been illustrated in **Figure 7**. It can be observed from the figure that a reduced angle between the stator winding flux and stator winding current vector can reduce the rotor current magnitude. It can be extracted from (12) and **Figure 7** that rotor current magnitude can be reduced by orienting it with the stator current in the event of a fault. The control structure for RSC switches from the conventional scheme to RRCOS during the fault event and is decided by the transient control switching algorithm [18], (Refer **Figure 2**). A detailed analysis has been explained in [18]. It is also extracted from [18] that the rotor current orientation further improves the transient voltage rise associated with rotor emf and DC-link voltage.

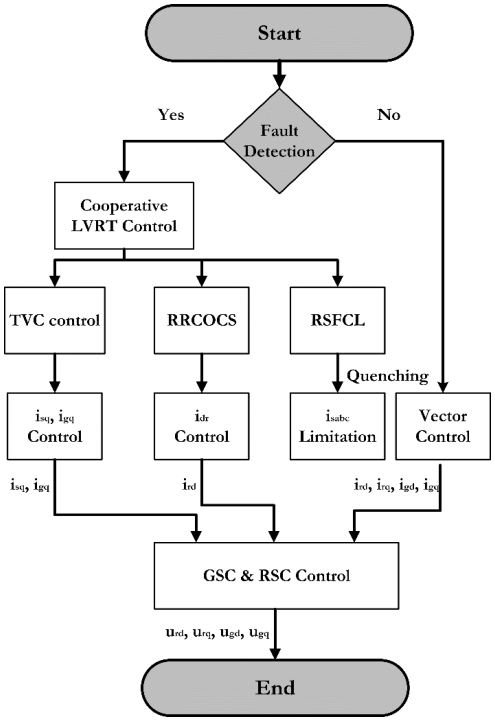

Figure 8 Control switching algorithm between normal and fault operation.

Results and discussion

The proposed control strategy is tested on the system given in section 3 and represented in **Figure 3**. The Control strategy switches between normal and faults operating conditions according to the flow chart defined in **Figure 8**. The performance of the proposed cooperative LVRT method is evaluated under a 3-phase symmetric fault condition with a grid voltage sag level of 0.99 at t = 0.0835 s which lasts for 100 milliseconds. The symmetric 3-phase to a ground fault has been considered in this paper for the performance evaluation due to its maximum severity. Three test conditions based on different control strategies have been investigated in this paper for the performance comparison, namely, Case A: Only with RRCOCS; Case B: With RRCOCS and TVC; and the proposed test Case C: With R-SFCL, RRCOCS, and TVC. Cases A and B are considered to be software LVRT control of DFIG whereas in test case C, software and hardware control are combined to have an advantage of both the control strategies. Also, the requirement of SFCL resistance (R_{max}) reduces for the proposed test case C to bring a similar improvement in voltage at Bus 1 compared to SFCL acting alone. The R-SFCL resistance requirement in test Case C is just 8 milliohms compared to 16 milliohms required when an R-SFCL operates alone to achieve a similar terminal voltage improvement [32]. The minimum terminal voltage profile for different (R_{max}) with R-SFCL acting alone and with R-SFCL & RRCOCS-TVC together is shown in **Figure 9**.

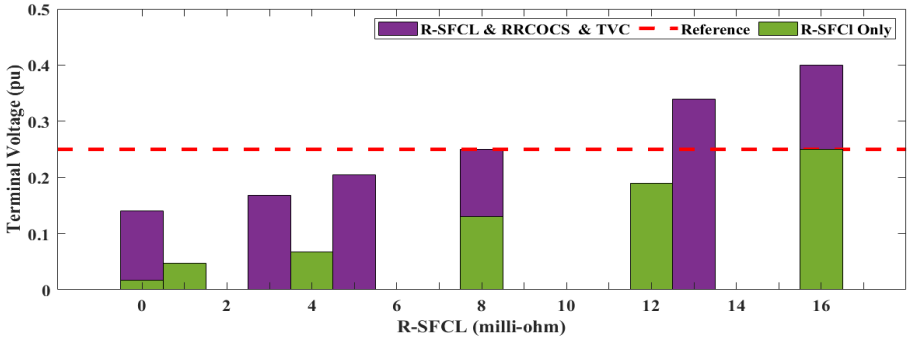

Figure 9 Terminal Voltage for different R-max with R-SFCl alone and with R-SFCL& RRCOCS-TVC.

As far as the DFIG terminal voltage is maintained at rated (1.0 p.u.) level, the reference values of the critical parameters i.e., the electromagnetic torque, dc bus voltage and, rotor currents are well tracked by the conventional vector control structure and are within the safe limits. However, during the fault event, the controller performance gets deteriorated and the critical parameters cross the safe limits and undergo transient oscillations. The simulation results presented in this section describe and compare the behavior of the critical parameters for different test cases. Additionally, the performance comparison of the variables is logged in **Table 2**.

Table 2 Performance comparison between different test cases.

System dynamic variables	Test - case A	Test - case B	Test - case C
Electromagnetic torque peak (pu)	2.30	2.40	1.80
Dc-link voltage peak (pu)	1.59	1.38	1.10
Reactive power generation (pu)	0	0.078	0.139
Terminal voltage RMS (pu)	0.04	0.09	0.26
Peak - Grid current (pu)	4.38	4.65	2.76
Peak - Rotor current(pu)	4.07	4.15	1.90

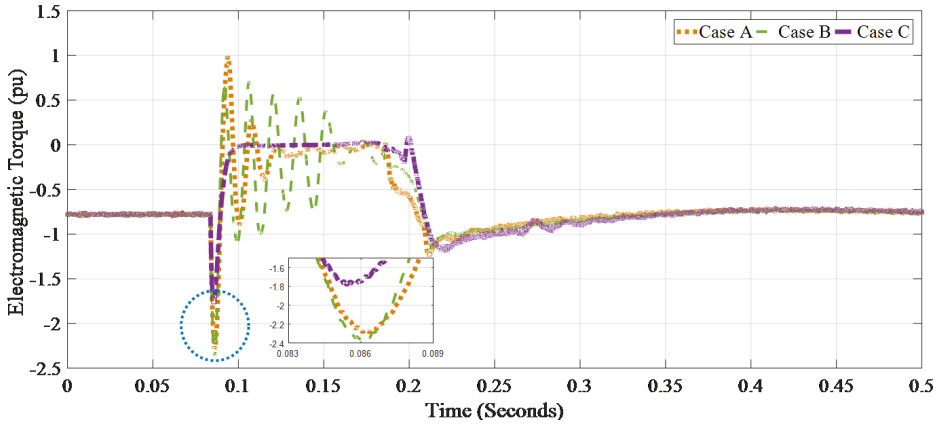

Figure 10 Electromagnetic torque response of DFIG.

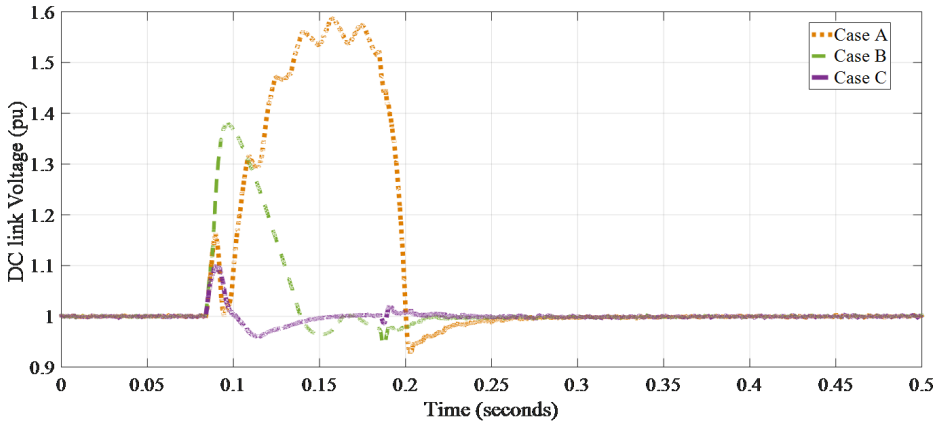

Figure 11 DC bus voltage response of DFIG.

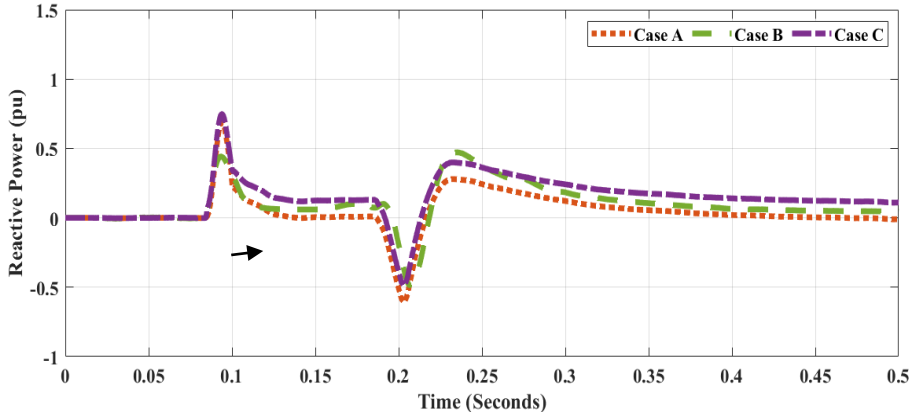

Figure 12 DFIG reactive power contribution with different test cases.

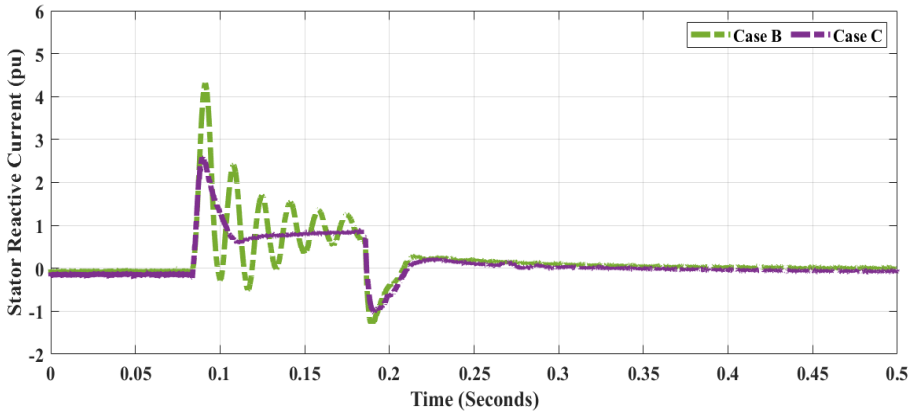

Figure 13 Stator reactive current injection with different test cases.

The electromagnetic torque behavior for a 3-phase symmetric fault is presented in **Figure 10**. The peak value of the electromagnetic torque reaches (~2.3 p.u.) and (~2.4 p.u.) for case A and B, respectively. However, it is limited to 1.8 p.u. with the proposed control strategy termed as case C and is below the maximum permitted value (2.0 p.u.) [31]. Also, the oscillations in electromagnetic torque get smoother in case C, compared to case A and B. This can prevent the mechanical system from vibrations, reduce the mechanical stress on them, and increase their life span.

The response of DC-link voltage has been shown in **Figure 11**. With RRCOCS in case A, the dc bus voltage peak goes to (~1.59 p.u.), surpassing the permissible safe limit (1.2 p.u.) [33]. Through the addition of TVC in case B, excess energy available with the dc bus capacitor can be used for reactive power generation through RSC and GSC. And hence the dc-link voltage peak reduces to 1.38 p.u. However, with the deployment of SFCL in case C, the dc bus voltage peak is further restricted to 1.1 p.u.

The reactive power control using TVC is illustrated in **Figure 12**. With RRCOCS alone in case-A, no reactive power is generated by the DFIG. With TVC activated in case B the stator and GSC are able to inject the reactive current of (~0.808 p.u) and (~0.195 p.u.) respectively as shown in **Figured 13** and **14**. However, the reactive power is restrained to (~0.078 p.u.) because of the low voltage at the grid terminal (Refer **Figure 12**). In Case C with the cooperative control scheme, the DFIG is able to output (~0.139 p.u.) of reactive power. Moreover, the oscillations in the injected stator and GSC reactive currents are also reduced (see **Figure 13** and **14**).

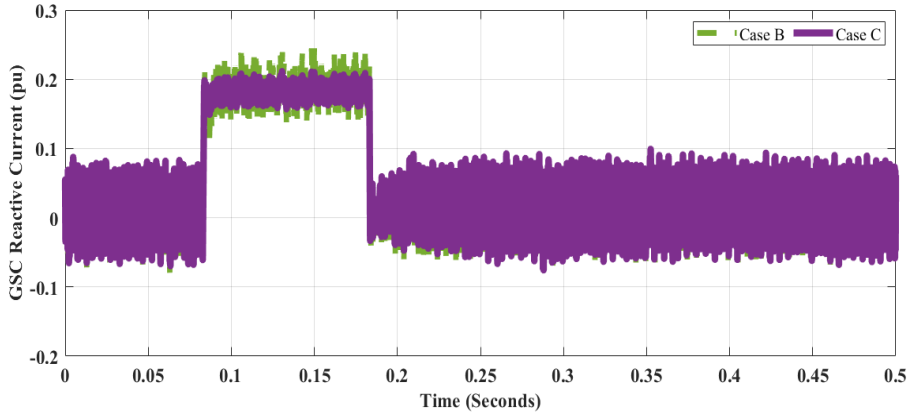

Figure 14 GSC reactive current injection with different test cases.

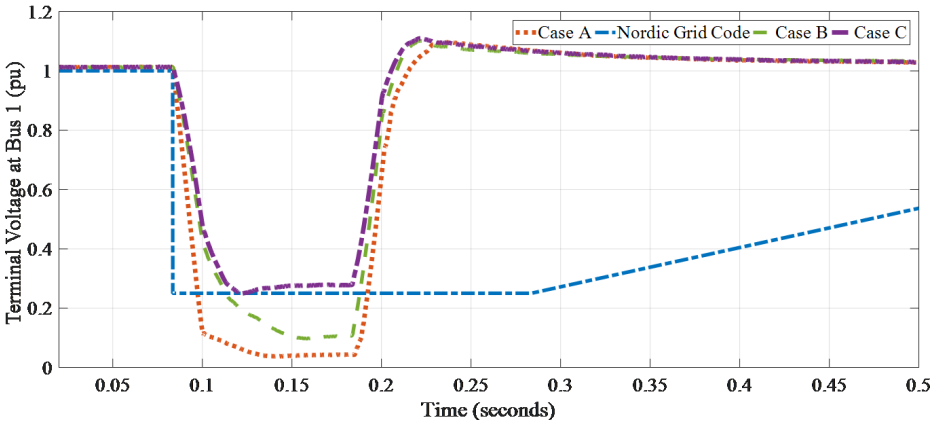

Figure 15 The terminal voltage at bus 1 under 3-phase fault.

Figure 15 reveals that with the RRCOCS only, the DFIG experiences a low terminal voltage close to (~0.04 p.u.) during the fault duration. In case B, the TVC contributes to a small reactive power generation by DFIG, and the terminal voltage gets improved to (~0.09 p.u.). When the SFCL, TVC, and RRCOCS are applied together in case C, the minimum voltage at the terminal is enhanced to (~0.26 p.u.) fulfilling the Nordic grid requirements [11].

Figures 16 - 18 show the responses of rotor current of the DFIG under case A - C, respectively. The RRCOCS scheme has limited ability to perk up the ride-through performance of DFIG amid a deep voltage sag. The rotor peak current values in case A and B can only be restricted to (~4.07 p.u.) and (~4.15 p.u.), respectively. These current levels are beyond the permissible value (2.0 p.u.) [31]. In case C, the SFCL supports to improve the wind farm voltage at the terminal, hence the rotor current peak value is further suppressed to (~1.9 p.u.). The grid current plots for different test cases are illustrated in **Figures 19 - 21.** Similar to rotor currents, the peak grid currents dynamics in test case A and B are very high (~4.38 p.u.) and (~4.65 p.u.), respectively. However, with the proposed test case C, the grid current peak is suppressed to (~ 2.69 p.u.).

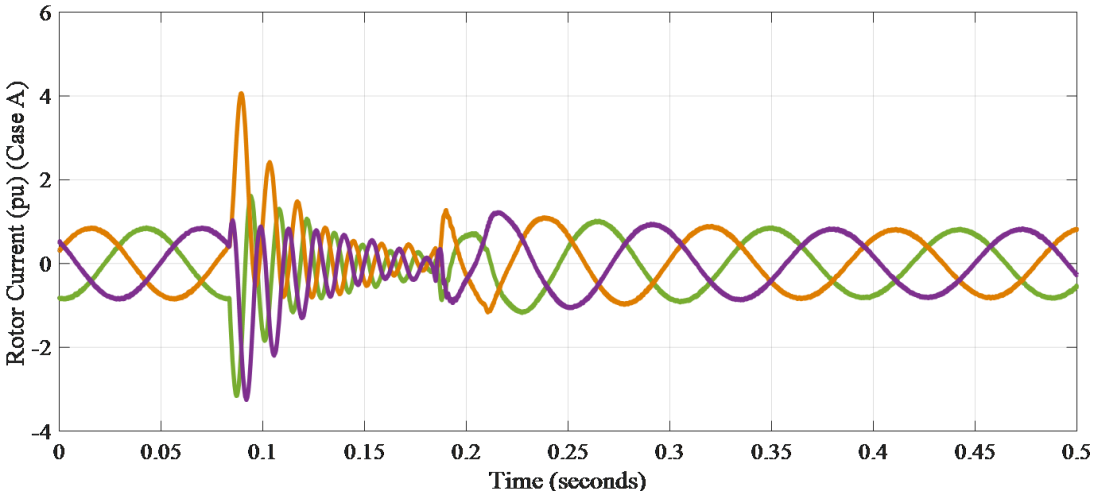

Figure 16 DFIG rotor winding currents (case A).

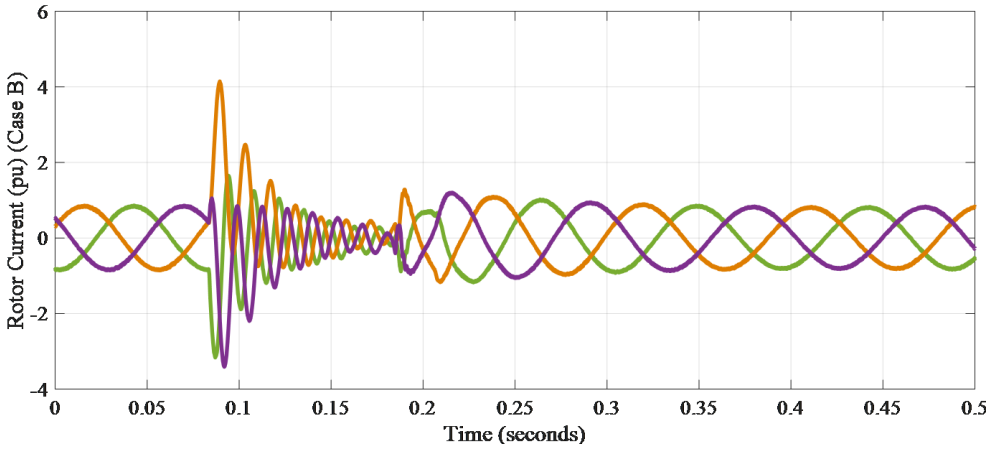

Figure 17 DFIG rotor winding currents (case B).

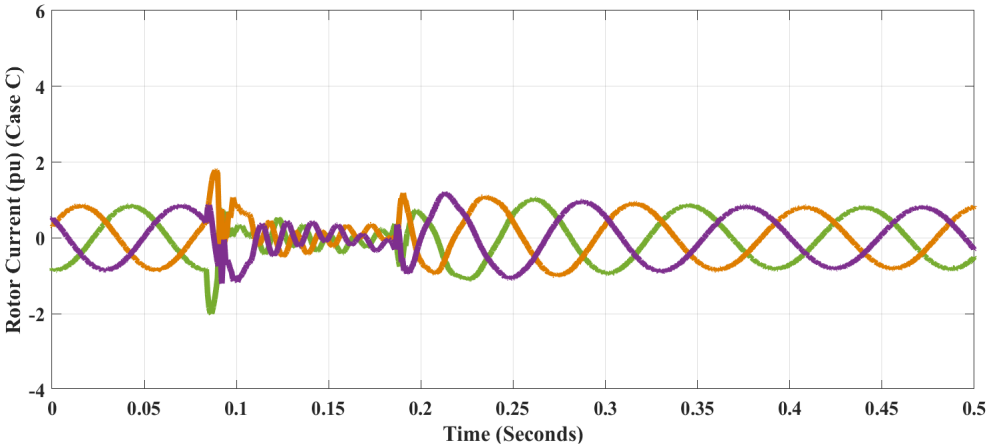

Figure 18 DFIG rotor winding currents (case C).

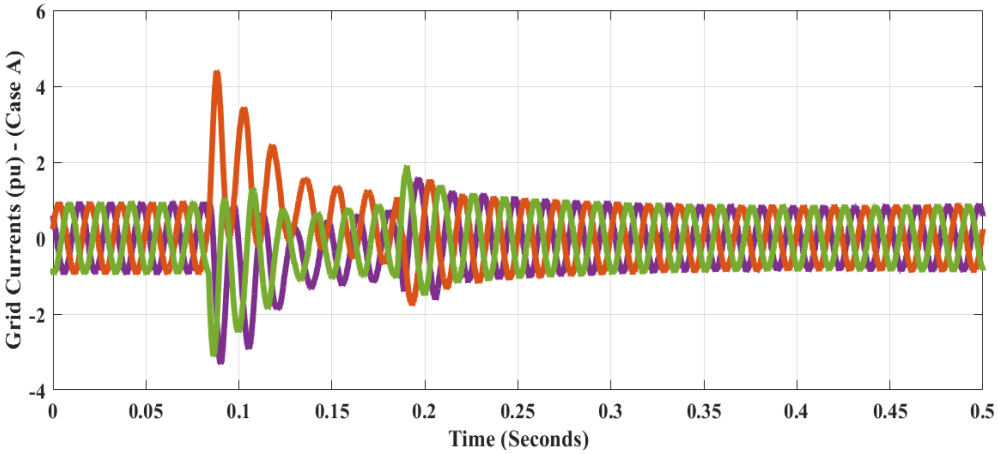

Figure 19 Three-phase grid currents (case A).

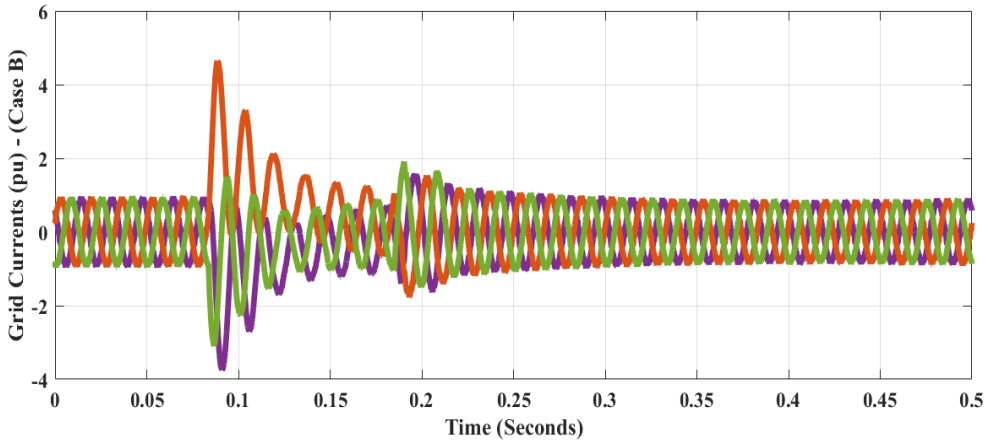

Figure 20 Three-phase grid currents (case B).

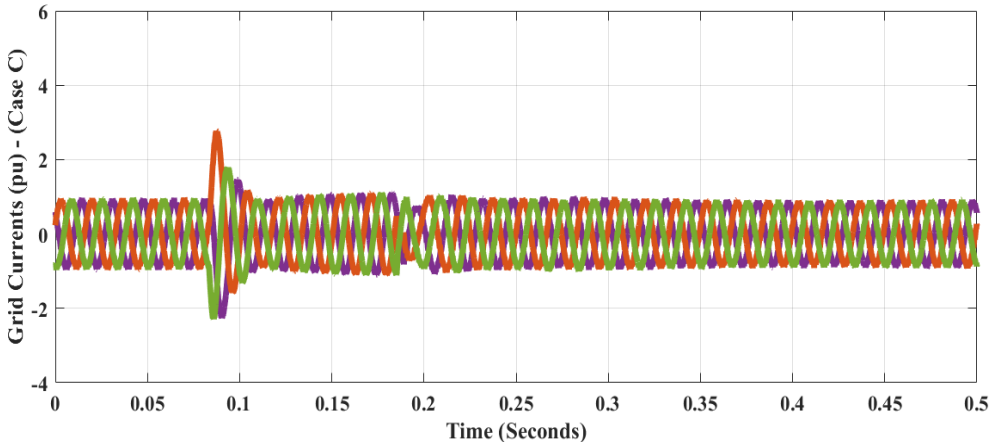

Figure 21 Three-phase grid currents (case C).

Conclusions

A new cooperative scheme merging the hardware circuit and software solution has been proposed in this paper for maintaining the LVRT requirement. In this cooperative scheme, the hardware solution is implemented using R-SFCL and the software solution through RRCOCS-TVC. The cooperative control strategy is being tested on the system given in **Figure 3** for 3 test cases A - C. Test case A analyzes the contribution of RRCOCS in the rotor current limitation. With the inclusion of TVC with RRCOCS, the reactive current control along with the rotor current limitation is achieved in test case B. In the proposed cooperative strategy in test case C, the voltage at the wind generator bus terminal is improved to satisfactorily meet the specified utility grid code at a reduced rating of R-SFCL resistance as compared with the R-SFCL control alone. Further, R-SFCL limits the rotor current in an indirect manner. The proposed scheme extracts the features of RRCOCS, TVC, and R-SFCL together. From the test result, the effectiveness of the proposed method is established in terms of the electromagnetic torque, rotor current, and dc bus voltage under severe fault conditions. This further improves the thermal performance of SFCL and enhances its recovery characteristics. The proposed cooperative scheme results in the reduction of SFCL rating, thermal improvement, and reverse recovery improvement. These improvements will certainly participate in compensating the dynamics under recurring faults and are needed to be explored. Also, the proposed cooperative LVRT control in this paper assumes homogeneous quenching of the R-SFCL deployed on the 3 phases. The impact of inhomogeneous quenching among 3 sets of R-SFCLis still unexplored.

References

[1] S Müller, M Deicke and RWD Doncker. Doubly fed induction generator systems for wind turbines. *IEEE Ind. Appl. Mag.* 2002; **8**, 26-33.

[2] J López, E Gubía, P Sanchis, X Roboam and L Marroyo. Wind turbines based on doubly fed induction generator under asymmetrical voltage dips. *IEEE Trans. Energ. Convers.* 2008; **23**, 321-30.

[3] AH Kasem, EF El-Saadany, HH El-Tamaly and MAA Wahab. An improved fault ride-through strategy for doubly fed induction generator-based wind turbines. *IET Renew. Power Generat.* 2008; **2**, 201-14.

[4] SQ Bu, W Du, HF Wang and S Gao. Power angle control of grid-connected doubly fed induction generator wind turbines for fault ride-through. *IET Renew. Power Generat.* 2013; **7**, 18-27.

[5] M Rahimi and M Parniani. Efficient control scheme of wind turbines with doubly fed induction generators for low-voltage ride-through capability enhancement. *IET Renew. Power Generat.* 2010; **4**, 242-52.

[6] Z Din, J Zhang, Z Xu, Y Zhang and J Zhao. Low voltage and high voltage ride-through technologies for doubly fed induction generator system: Comprehensive review and future trends. *IET Renew. Power Generat.* 2021; **15**, 614-30.

[7] FKA Lima, A Luna, P Rodriguez, EH Watanabe and F Blaabjerg. Rotor voltage dynamics in the doubly fed induction generator during grid faults. *IEEE Trans. Power Electron*. 2010; **25**, 118-30.

[8] Z Din, J Zhang, Y Zhu, Z Xu and A El-Naggar. Impact of grid impedance on LVRT performance of DFIG system with rotor crowbar technology. *IEEE Access* 2019; **7**, 127999-8008.

[9] Z Din, J Zhang and Z Xu. A review on low voltage ride-through for DFIG based wind turbines. *In*: Proceedings of the PCIM Asia 2018; International Exhibition and Conference for Power Electronics, Intelligent Motion, Renewable Energy and Energy Management, Shanghai, China. 2018.

[10] J Hu, Y Huang, D Wang, H Yuan and X Yuan. Modeling of grid-connected DFIG-based wind turbines for dc-link voltage stability analysis. *IEEE Trans. Sustain. Energ.* 2015; **6**, 1325-36.

[11] M Tsili and S Papathanassiou. A review of grid code technical requirements for wind farms. *IET Renew. Power Generat.* 2009; **3**, 308-32.

[12] R Bhushan and K Chatterjee. Mathematical modeling and control of DFIG-based wind energy system by using optimized linear quadratic regulator weight matrices. *Int. Trans. Electr. Energ. Syst.* 2017; **27**, 1-23.

[13] SA Taher, ZD Arani, M Rahimi and M Shahidehpour. A new approach using combination of sliding mode control and feedback linearization for enhancing fault ride through capability of DFIG-based WT. *Int. Trans. Electr. Energ. Syst.* 2018; **28**, e2613.

[14] S Li, J Huang and T Sun. Analytical LVRT analysis of doubly fed induction generator with MPC-based DSCC/DRCC. *IET Renew. Power Generat.* 2019; **13**, 2462-71.

[15] L Zhou, J Liu and S Zhou. Improved demagnetization control of a doubly-fed induction generator under balanced grid fault. *IEEE Trans. Power Electron.* 2015; **30**, 6695-705.

[16] S Xiao, G Yang, H Zhou and H Geng. An LVRT control strategy based on flux linkage tracking for DFIG-based WECS. *IEEE Trans. Ind. Electron.* 2013; **60**, 2820-32.

[17] D Zhu, X Zou, L Deng, Q Huang, S Zhou and Y Kang. Inductance-emulating control for DFIG-Based wind turbine to ride-through grid faults. *IEEE Trans. Power Electron.* 2017; **32**, 8514-25.

[18] W Teng and Y Meng. Rotor-reference-current-oriented control strategy for low-voltage ride-through of DFIG. *IEEJ Trans. Electr. Electron. Eng.* 2018; **17**, 61-71.

[19] D Xie, Z Xu, L Yang, J Ostergaard, Y Xue and KP Wong. A comprehensive LVRT control strategy for DFIG wind turbines with enhanced reactive power support. *IEEE Trans. Power Syst*. 2013; **28**, 3302-10.

[20] J Morren and SWHD Haan. Ridethrough of wind turbines with doubly-fed induction generator during a voltage dip. *IEEE Trans. Energ. Convers*. 2005; **20**, 435-41.

[21] KE Okedu, SM Muyeen, R Takahashi and J Tamura. Wind farms fault ride through using DFIG with new protection scheme. *IEEE Trans. Sustain. Energ*. 2012; **3**, 242-54.

[22] W Qiao, R Harley and G Venayagamoorthy. Coordinated reactive power control of a large wind farm and a STATCOM using heuristic dynamic programming. *In*: Proceedings of the 2009 IEEE Power & Energy Society General Meeting, Alberta, Canada. 2009.

[23] C Wessels, F Gebhardt and FW Fuchs. Fault ride-through of a DFIG wind turbine using a dynamic voltage restorer during symmetrical and asymmetrical grid faults. *IEEE Trans. Power Electron.* 2011; **26**, 807-15.
[24] H Mohammadpour, SG Zadeh and S Tohidi. Symmetrical and asymmetrical low-voltage ride through of doubly-fed induction generator wind turbines using gate controlled series capacitor. *IET Renew. Power Generat.* 2015; **9**, 840-6.
[25] U Chaudhary, P Tripathy and SK Nayak. Application of bridge-type FCL for betterment of FRT capability for DFIG-based wind turbine. *In*: Proceedings of the 2014 6th IEEE Power India International Conference, Delhi, India. 2014.
[26] M Firouzi. A modified capacitive bridge-type fault current limiter (CBFCL) for LVRT performance enhancement of wind power plants. *Int. Trans. Electr. Energ. Syst.* 2018; **28**, e2505.
[27] Z Din, J Zhang, Z Xu, Y Zhang and J Zhao. Realization of fault ride through for doubly fed induction generator system with cascade converter. *Int Trans. Electr. Energ. Syst.* 2021; **31**, e12792.
[28] Z Din, J Zhang and Y Jiang. Doubly fed induction generator with cascade converter for improving dynamic performances. *In*: Proceedings of the 2018 IEEE Energy Conversion Congress and Exposition, Oregon. 2018.
[29] W Uddin, K Zeb, A Tanoli and A Haider. Hardware-based hybrid scheme to improve the fault ride through capability of doubly fed induction generator under symmetrical and asymmetrical fault. *IET Generat. Transm. Distrib.* 2018; **12**, 200-6.
[30] X Xiao, R Yang, X Chen, Z Zheng and C Li. Enhancing fault ride-through capability of DFIG with modified SMES-FCL and RSC control. *IET Generat. Transm. Distrib.* 2018; **12**, 258-66.
[31] ZC Zou, XY Xiao, YF Liu, Y Zhang and YH Wang. Integrated protection of DFIG-based wind turbine with a resistive-type SFCL under symmetrical and asymmetrical faults. *IEEE Trans. Appl. Supercond.* 2016; **26**, 1-5.
[32] R Ou, XY Xiao, ZC Zou, Y Zhang and YH Wang. Cooperative control of SFCL and reactive power for improving the transient voltage stability of grid-connected wind farm with DFIGs. *IEEE Trans. Appl. Supercond.* 2016; **26**, 1-6.
[33] YW Shen, DP Ke, YZ Sun, DS Kirschen, W Qiao and XT Deng. Advanced auxiliary control of an energy storage device for transient voltage support of a doubly fed induction generator. *IEEE Trans. Sustain. Energ.* 2016; **7**, 63-76.